Dual sensitization enhancement in cavity optomechanics for ultra-high resolution temperature sensing

Yize Liu, Junfeng Jiang, Kun Liu, Shuang Wang, Panpan Niu, Tong Wang, Tianhua Xu, Xuezhi Zhang, and Tiegen Liu

***Abstract*—As a basic physical parameter, temperature plays an important role in science and industry areas. The cavity optomechanics especially the spring effect provide an ideal platform for precision measurement. Here, we bridge between optical sensitization and optomechanical transduction by fabricating a liquid-core microbubble resonator to realize dual sensitization enhancement. The high thermo-optic coefficient liquid is injected into the microbubble to increase the temperature sensitivity of optical resonant peak shift. The optomechanical spring effect is used to transduce the amplified optical shift to mechanical frequency change and further enhance the temperature response. Through the enhancement combination of optical and mechanical methods, we have achieved a sensitivity of 8.1 MHz/°C, which is at least two orders of magnitude higher than traditional optomechanical approaches. The temperature resolution is estimated as high as 5.3×10^{-5} °C with mechanical frequency linewidth 8.6 kHz. A capillary ethanol evaporation experiment is constructed to demonstrate capability of the tiny temperature fluctuations measurement. The novel dual approach greatly enhanced the ultra-high resolution sensing capability and have a flexible sensitivity adjust potential with simply injecting different liquids.**

***Index Terms*—fiber optics sensors, optomechanics, WGM, temperature measurement**

I. Introduction

High resolution temperature measurement is essential for many applications ranging from biomedical research [1-3], energy storage battery health monitoring [4], earth science [5] ocean investigation [6], to space exploration [7]. For example, temperature measurement in space-borne gravitational wave observatory requires noise equivalent temperature level be less than 10^{-5} K $Hz^{-1/2}$ to ensure extreme weak gravitational wave signal detection [8, 9], which corresponding to a temperature resolution 1.7×10^{-6} °C under 29 mHz bandwidth. The detection of the liquid helium specific heat also proposes ultra-high temperature resolution requirements (approximately 3×10^{-8} °C) in the region of 22×10^{-3} °C [10, 11]. Optical sensing technology is a promising candidate for thermal sensing due to their high sensitivity, miniaturization, and low cost. Especially, the resonance of optical microcavities [12] greatly enhances the light-matter interaction, thus improving the sensing resolution. Temperature affects the cavity optical resonance [13] through refractive index and geometric size and reflects as a spectrum line shift of optical resonant mode, the resolution depends critically on the optical quality factor Q_o (determining minimal detectable optical cavity resonance shift) and temperature sensitivity [14]. To improve the sensing resolution, a lot of works were dedicated to increase the temperature sensitivity. Organic materials (PDMS, PMMA et al.) with large thermal expansion coefficient are frequently chosen to form smooth solid microcavities and improve sensitivity [15, 16]. Liquid or liquid-core microcavities are also formed to make use of their high thermo-optical coefficient [17-19]. However, the accompanied optical Q_o deterioration in these microcavities will offset the sensitivity improvement. The former highest estimated resolution is ~10^{-4} °C and the latter is ~10^{-3} °C. Thus, the resolving power is still close to that of the simple silica microcavity [20].

In recent decades, the cavity optomechanics is introduced into high precision sensing [21-23]. Temperature sensitivity of 0.0065 MHz/°C had been demonstrated with a microdisk oscillator [24]. Optomechanical microbubble sensor with copper substrate achieved 0.0113 MHz/°C and an estimated temperature resolution ~10^{-4} °C [25]. However, these optomechanical sensors only rely on the mechanical oscillation frequency shift derived from the effective mass disturbance or the intrinsic mechanical spring constant change, while optical part only provides readout function. The resolution is determined by the effective mechanical quality factor Q_{meff} and the temperature sensitivity. Furthermore, fixing the detuning between pump laser and resonance is a common solution to avoid the impact of optical mode changes on mechanical frequency, which be realized by increasing cavity wall thickness to suppress the optical resonance wavelength shift [26] or tracking pump laser wavelength to the resonance wavelength shift [27]. However, a larger wall thickness will

This work was supported by National Instrumentation Program of China (Grant No. 2022YFF0706000); National Natural Science Foundation of China (Grant No. 61735011, U2006216); and the open project of Key Laboratory of Opto-electronics Information Technology (Grant No. 2022KFKT004, 2022KFKT005); the open project of Key Laboratory of Micro Opto-electro Mechanical System Technology (Grant No. 2022KFKT006). *(Corresponding authors: Junfeng Jiang.)*

The authors are with the School of Precision Instruments and Opto-Electronics Engineering, and Tianjin Optical Fiber Sensing Engineering Center, Institute of Optical Fiber Sensing, China, and Key Laboratory of Opto-electronics Information Technology, Tianjin University, Tianjin 300072, China. T. Xu is also with the School of Engineering, University of Warwick, Coventry, United Kingdom CV47AL. (e-mail: liu_yize@tju.edu.cn; jiangjfjxu@tju.edu.cn; beiyangkl@tju.edu.cn; shuangwang@tju.edu.cn; niupanpan@tju.edu.cn; wangtong1994@tju.edu.cn; xutianhua@tju.edu.cn; zhangxz@tju.edu.cn; tgliu@tju.edu.cn).

decrease the sensitivity of mechanical modes [28] and real time precise pump laser tuning is difficult in practical application. The optical spring effect in cavity optomechanics [29, 30], which is sensitively related to laser-cavity detuning, has developed into another detection mechanism. Circulating optical power in cavity can generate optical spring constant and change the mechanical resonance frequency consequently. The transduction and amplification between laser-cavity detuning and optomechanical oscillation frequency shift redefine the Q_{om} value, which is $Q_{om}=Q_oQ_{meff}$ [30]. Despite this advantage in minimal shift detectable ability, optomechanical spring effect sensing just reported in solid silicon-based microresonator, which focusing on optical and mechanical transduction while neglecting the potential of optical sensitization. Moreover, solid microcavity cannot provide flexible and simple sensitivity adjustment capability.

In this paper, we introduce a liquid core microbubble temperature sensor with dual sensitization enhancement based on optomechanics spring effect. By injecting high thermo-optic coefficient liquid inside the microbubble cavity, the temperature response of optical resonance is amplified. Furthermore, the spring effect dramatically amplifies the cavity optical resonance shift induced by temperature and transduces it into the optomechanical oscillation frequency change. This is different from previous optomechanical temperature sensors mainly based on phonon laser phenomena. Although the blue-tuned pump laser is used to decrease overall mechanical damping rate and achieve narrow linewidth, the dominant cavity optomechanical influence is the optical spring effect. This dual sensitization enhanced liquid core optomechanical cavity achieved a sensitivity of 8.1 MHz/°C, which is at least two orders of magnitude higher than that of traditional optomechanical approach. Injecting liquids with different thermal optical coefficients will provide a new degree of freedom to regulate temperature sensitivity. Finally, the small temperature changes caused by the convex ethanol meniscus evaporation on a microtube end is measured to demonstrate the practical temperature resolving ability of the sensor system.

II. Results

A. The fabrication of liquid core silica microbubble

The silica microbubble is prepared by melting and pressurizing the commercial fused silica microcapillary (TSP250350, Polymicro Inc.). In the first step, the internal injection pressure microcapillary is heated with a centimeter-sized oxyhydrogen flame and stretched axially to reduce the radius and wall thickness. The second step is to heat the stretched microcapillary with a millimeter-sized flame. At the same time, a syringe is used to inject a certain volume of air into the capillary to help it expand into microbubble. Through the control of pressure and stretch length, we can obtain microbubble with expected radius and wall thickness. The fabrication details can be found in our previous work [31]. The liquid core microbubbles are realized by filling with chosen solution by a syringe. According to the usage requirements, the separate microcavity or both the microcavity and taper fiber can be fixed on a glass substrate by UV glue. This packaged method has good mechanical stability [32].

B. The dual sensitivity enhancement principle of microbubble optomechanics

A continuous-wave pump laser is evanescently coupled into the cavity whisper gallery mode (WGM) and produces a radiation pressure to deform the cavity, as shown in Fig. 1(a). The wall is oscillated mechanically in a similar form as a spring at natural mechanical modes and in turn modulates the optical cavity resonance (radiation pressure). This unique dynamic backaction [33] in optomechanics is a modification of mechanical dynamics caused by the radiation pressure of light and finite cavity decay time. We use blue tuning of pump to realize the amplification. It is important to note that the blue detuning decrease the effective mechanical damping rate and increases Q_{meff} [34, 35].

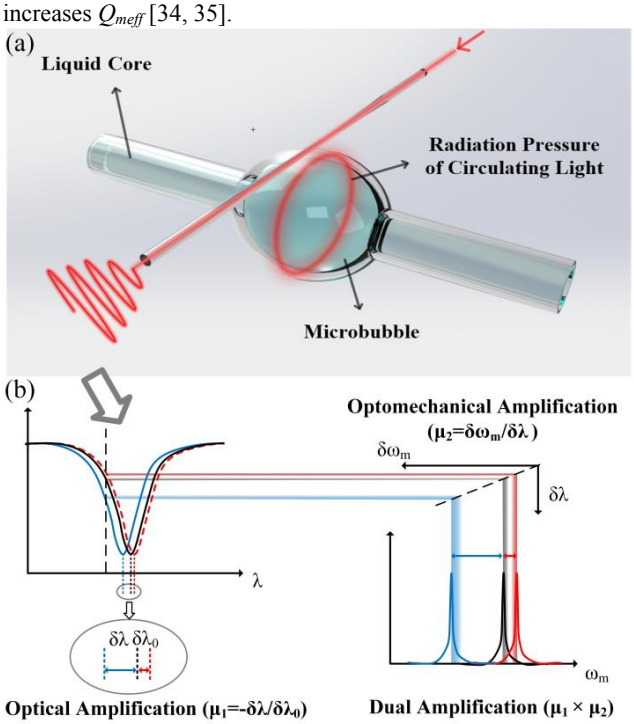

Fig. 1. Schematic diagram of temperature sensing. (a) Schematic diagram of optomechanical oscillation. (b) Schematic diagram of the dual sensitivity enhancement principle (temperature rises). The left inset shows the WGM spectrum, and the right inset is the mechanical oscillation spectrum due to optomechanical interaction. The black lines represent the original WGM and mechanical oscillation spectrum of hollow microcavity. The red lines represent the WGM and mechanical oscillation frequency shift of hollow microcavity. The blue lines represent the WGM and mechanical oscillation frequency shift of acetone core microcavity.

The schematic diagram of dual sensitivity enhancement temperature sensing is shown in Fig. 1(b). When the temperature fluctuates slightly in the surroundings, the cavity optical resonance mode wavelength will shift and change the pre-setting detuning. The optical resonance shift $\delta\lambda_0$ is determined by the thermo-optic and thermal expansion effects

[17]. The silica microbubble thermal sensor has a small sensitivity ~6 ppm/°C [13]. But the optical amplification $\mu_1 = |\delta\lambda / \delta\lambda_0|$ increases with larger absolute value of thermo-optical coefficient liquid for the liquid-core microbubble (see APPENDIX A for more details). The mechanical frequency depends sensitively on the laser-cavity detuning, therefore the detuning is transduced to a mechanical frequency shift $\delta\omega_{m0}$. This optomechanical amplification $\mu_2 = \delta\omega_m / \delta\lambda$ arise from the optical spring effect [29, 30], which means that the effective rigidity of microcavity is also modified by the optical detuning (see APPENDIX B for more details). In summary, the high thermo-optical coefficient liquid core amplifies the optical resonance shift. Then, the spring effect transduces the detuning to the mechanical frequency shift and achieves another amplification. The two effects provide a dual amplification factor $\mu_1 \times \mu_2$.

C. *The optical enhancement of liquid core microbubble*

The temperature response of optical mode is characterized by the common WGM sensing system. The light from a tunable laser (Keysight 81607A) is coupled into the liquid core microbubble through a tapered fiber to excite WGM, the transmitted light is collected by a powermeter (Keysight 81636B). The tunable laser is scanned to measure the transmission WGM spectrum. The microbubble with a radius of 146.4 μm is placed above a heating station with temperature controller. The liquid core material is acetone and its thermo-optic coefficient is k_{core} =-5×10^{-4}/°C. The transmission spectrum was recorded with temperature changing from 25 °C to 25.5 °C with step 0.1 °C, as shown in Fig. 2(a). The resonant wavelength is blue shift and changed linearly with temperature. The optical *Qo* (calculated as $Qo=\lambda/\Delta\lambda$, where $\Delta\lambda$ is the linewidth of the resonant peak) is 2.2×10^5 and keeps stable during the whole process. Fig. 2(b) shows the optical temperature response S_{TO} is 41.2 pm/°C, which provide optical amplification μ_1 =4.44. The temperature resolution of sensors can be calculated as $\Delta T_r = R_s / S_T$, where S_T is the temperature sensitivity and R_s is the spectral resolution. The spectral resolution is defined as FWHM/20 [15, 19, 36] and the estimated temperature resolution using optical WGM spectrum line is only R_{TO}=8.5 × 10^{-3} °C. Other higher thermo-optic coefficient liquid materials can be chosen as liquid cores to further improve the sensitivity, such as cholesteric liquid crystals or cyclohexane.

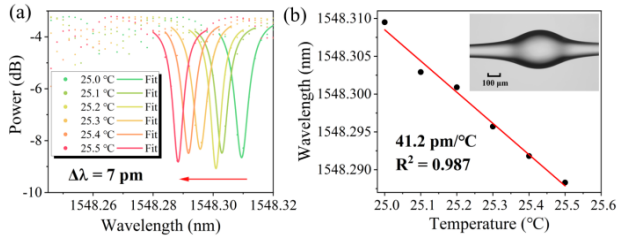

Fig. 2. The temperature response of optical WGM mode. (a) Transmission optical WGM spectra at the different temperatures. (b) Center wavelength evolution of the liquid core microbubble versus temperature change. Inset: optical microscopic image of the liquid core microbubble.

D. *The spring effect and optomechanical enhancement of liquid core microbubble*

The same tunable laser is then set with a fixed wavelength and power 6 mW. The taper fiber is contacted to the microbubble surface to reduce the possible influence of external mechanical instability disturbance. The addition of mechanical damping by contact is small enough to be neglected [37]. A large bandwidth photodetector (Thorlabs PDB450C) and an electrical spectrum analyzer (Agilent N9010A) to observe the mechanical oscillation frequency spectrum. When the pump laser wavelength is blue detuned with the optical WGM resonant peak, optomechanical oscillation can be excited. Fig. 3(a) shows the typical radial breathing mechanical motion frequency spectrum of the acetone core microbubble when the detuning is -3.4 pm. There are two fundamental mechanical modes can be identified at 2.97 MHz and 3.83 MHz, which may be resulted from the nonideal symmetric shape of microbubble. The high-order mode frequency components are resulted from the nonlinear transduction of the optical cavity [22]. The mechanical eigenmode with frequency of 3.83 MHz and a higher SNR 9.4 dB is chosen for sensing. Its linewidth is narrow to 8.664 kHz, corresponding to an effective mechanical Q_{meff} of 442.

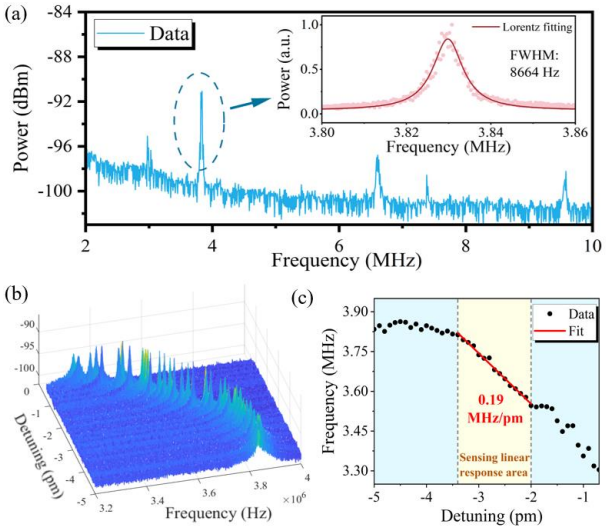

Fig. 3. The optomechanical oscillation versus laser cavity detuning. (a) An example of the optomechanical oscillation frequency spectrum. Inset: The fundamental mechanical mode. The center frequency is located at ~3.83 MHz, the FWHM is 8664 Hz. (b) Series of frequency spectrum for the fundamental mechanical mode when laser detuning from -5 pm to -0.8 pm (0.1 pm step), respectively. (c) Evolution of the measured mechanical resonant center frequency.

To experimentally determine the influence of spring effect resulting from the laser-cavity detuning, the input laser

wavelength is set away from the optical WGM resonance peak and then gradually approaches. In order to ensure blue detuning, the input laser wavelength is smaller than the resonance wavelength during the whole process. Fig. 3(b) illustrates the variation of the fundamental optomechanical oscillation mode with the detuning. It is obviously found that the optomechanical oscillation signal first enhances and then impairs with the detuning change. The mechanical linewidth changes also reflect the impact of detuning on the overall mechanical damping rate. More importantly, the detuning also affects the cavity spring coefficient, which is called the spring effect. Because the mechanical frequency is directly related to the spring coefficient, the detuning change bring the frequency change. The evolution of the center mechanical frequency is clearly demonstrated in Fig. 3(c). As the input laser approaches cavity resonance, the mechanical frequency shifts with detuning, which indicates the optical spring effect leads to an effective stiffness change. The mechanical frequency increases from 3.81 MHz to a peak value of 3.86 MHz, and then decreases quickly to about 3.3 MHz. There exists a good linear response at the laser-cavity detuning range -3.4 pm to -2 pm, the slope is -0.19 MHz/pm and represents the optomechanical amplification μ_2. This detuning range can also ensure the Q_{meff} being above 400.

E. The temperature response measurement

Based on the microbubble optical temperature sensitivity S_{TO} is 41.2 pm/°C and the spring effect transduce slope is -0.19 MHz/pm, the theoretical temperature sensitivity of dual amplification liquid core microbubble sensor is 7.83 MHz/°C. The resolution of the optical resonance wavelength shift detection method is R_{TO}=8.5×10^{-3} °C, which will be increased to the theoretical resolution 2.1 × 10^{-5} °C using mechanical frequency shift under dual sensitization.

In the temperature measurement experiment, the input laser wavelength is set at a detuning -3.4 pm of the resonant peak to make sure a good quality optomechanical oscillation and spring effect. The mechanical frequency shift with temperature is shown in Fig. 4. Limited by the temperature control device, the minimum temperature setting difference is 0.01 °C, the temperature is varied from 25.00 °C to 25.04 °C in 0.01 °C steps and each measurement is carried out after 1 min temperature stabilizing. When the temperature is below 25.03 °C, the detuning guarantee the spring effect still in the linear range. The linear fit shows a temperature sensitivity of 8.1 MHz/°C, which is close to the theoretical calculation value 7.83 MHz/°C. When the interaction between optical and mechanical modes in cavity optomechanics is not considered, the microbubble structure mechanical mode frequency also shifts with temperature. The microbubble breathing mode temperature response has been modeled in theory and read out through phonon laser phenomenon [25]. However, the temperature-dependent frequency shift of mechanical mode (the order of kHz/°C) is three orders of magnitude smaller than the cascade method and can be ignored. At 25.04 °C, the detuning is too large to enter nonlinear region and the mechanical frequency remains almost unchanged, as indicated from Fig. 3(c). In our system, the effective mechanical Q_{meff} is ~400. So, the estimated temperature resolution is 5.3×10^{-5} °C. The improved resolution also indicates that the spring effect-based temperature sensing method indeed redefines the minimum resolving power of the system.

A performance comparison between the proposed spring effect liquid core microbubble sensor and the other microcavity thermometers was listed in Table 1. Compared with other thermometers based on optomechanical oscillations, the proposed sensor has a large improvement in sensitivity. Although the silica microsphere sensor has a better resolution, its oscillation linewidth enters sub-Hertz regime which places high performance demands on frequency measurement instruments. In practical application, the high sensitivity will significantly facilitate the mechanical spectrum analysis by allowing to use frequency measurement instrument with a coarser resolution. Although the optical Q_o of proposed sensor is not very high, resolution improvement of at least one order of magnitude is obtained because dual sensitization enhances the minimal detectable capacity. For the liquid core microcavity WGM sensors, the measurable temperature range depends on the fluid in the core [17]; thus, for acetone this is limited from -94 °C to 56 °C. So, the thermo-optic tuning of WGM, namely optical amplification can be applied over a large temperature range. For optomechanical amplification, it is based on the laser-cavity detuning, especially the sensing linear response area shown in Fig. 3(b). Therefore, the reported resolution and response pertain to any 0.03 °C section within the range of -94 °C to 56 °C.

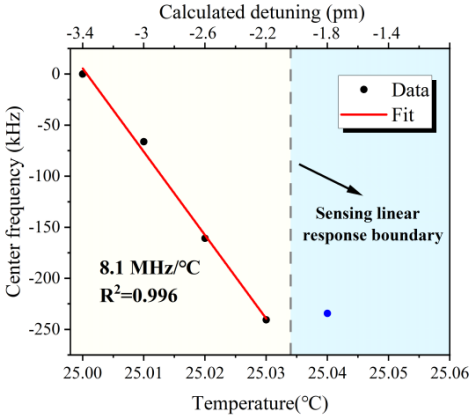

Fig. 4. The center frequency varies different temperatures.

TABLE I
Comparison of sensing features between the demonstrated spring effect temperature sensor and other WGM-based methods.

Principle	Structure	Sensitivity	Resolution (°C)	Ref
Optical resonance wavelength shift	Silica microsphere	13.4 pm/°C	1.1×10^{-3} °C	[20]

	Lithium niobate microdisk	6.67 pm/℃	8×10^{-4}	[38]
	PDMS microsphere	245 pm/℃	2×10^{-4}	[15]
	Dye-doped Oil Droplet	377 pm/℃	1.7×10^{-2} *	[18]
	Dye-doped LC droplet	1500 pm/℃	3.1×10^{-2} *	[39]
	Liquid crystal microdroplet	267.6 pm/℃	7.5×10^{-2}	[19]
	Liquid-core silica microbubble	200 pm/℃	8.5×10^{-3}	[17]
Mechanical frequency shift under opto-mechanics	Silica microsphere	6.5×10^{-3} MHz/℃	1.5×10^{-5} *	[24]
	Silica microbubble with copper substrate	1.13×10^{-2} MHz/℃	1×10^{-4}	[25]
Mechanical frequency shift under dual sensitization	Liquid-core silica microbubble	8.1 MHz/℃	5.3×10^{-5}	Ours

* The calculation results were estimated according to the optimal data in the references. The optical spectral or frequency spectral resolution is considered as one-twentieth of their resonant peak FWHM.

We construct a scenario of temperature changes caused by ethanol evaporation to demonstrate the practical temperature resolution of our sensors. Evaporation leads to a temperature drop at the liquid–vapour interface, and it is this reduction of temperature respect to the surrounding ambient that supplies the heat to sustain the phase change. Especially for a heat pipe, a fluid undergoes evaporation at one end due to heat being transferred into the heat pipe and condensation at the other end where heat is removed from the heat pipe. The high precision temperature measurement is crucial for analyzing Marangoni convection model and understand the dynamics process in this liquid motion [40-42]. The experimental layout is displayed in Fig. 5(a) (see APPENDIX C for more details). The acetone-core microbubble is single side fixed on the glass slide substrate to ensure stabilizing. The tapered fiber is located directly above the microbubble and perpendicular to the axial direction. A microtubule with an outer diameter of 310 μm, a wall thickness of 32 μm is placed near the microbubble. Additionally, the tube, connected to the injection pump and paralleled to the glass slide, has ethanol injected at a constant flow rate. The meniscus advances inside the tube till it reaches the tube end. Then, the meniscus pins itself to the tube end and gradually forms three kinds of shapes, namely: concave, flat, and convex [40, 43, 44]. Once the meniscus protrudes outside the tube, the pump is stopped and because of spontaneously continuous evaporation to open air, the meniscus retracts back inside the tube. During this process, the contact angle (shown in Fig. 5(b)) gradually decreases. Fig. 5(c) insets illustrate the variation of meniscus shape during one evaporation. The contact angle decreased from 69° to 0° and maintained for a few seconds.

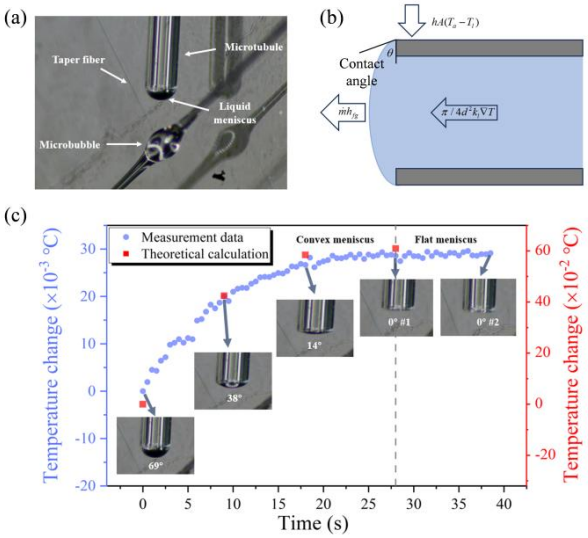

Fig. 5. The temperature change in ethanol evaporation process. (a) Experimental setup for temperature measurements with the use of spring effect sensor. (b) Capillary tube with heat paths. (c) Measured and theoretical calculation temperature changes over time. Insets: sequence of vertical optical images of meniscus interface showing changing meniscus shape.

The theoretical temperature difference can be evaluated through the energy balance. In steady state, the evaporation flux is equal the convective heat transfer term between the tube and the surrounding environment. The heat paths are shown in Fig. 5(b). Due to heat conduction in the liquid is of several orders of magnitude less that the heat coming from outside the tube [45], we ignore the term $\pi / 4d^2 k_l \nabla T$. So, the evaporation rate times the latent heat is equal the heat transferred from the ambient through the tube external surface via the base of the drop [42]:

$$mh_{fg} = hA(T_a - T_l) \tag{1}$$

where m is the evaporation mass rate, h_{fg} is the evaporation latent heat. h is the air–tube heat transfer coefficient. A is the external tube surface area, and can be calculated as $2\pi R \cdot 2R$. T_a is the ambient temperature and T_l is the liquid temperature, which can be regarded as constant at our system. Through the simplified model of a sessile drop [46], the convex ethanol meniscus evaporation mass rate in air reduces to:

$$-m = \pi RD(1-H)c_v(0.27\theta^2 + 1.30) \tag{2}$$

where $(1-H)c_v$ represent the vapor concentration difference, D is the diffusivity and θ is contact angle (radian value). Table 2 lists the theoretical temperature difference $T_a - T_l$ from Equation (1).

TABLE II

Theoretical temperature difference as a function of the contact angle computed from the model.

Contact angle (degree)	$T_a - T_l$ (°C)	Contact angle (degree)	$T_a - T_l$ (°C)

0	1.90253	40	2.10737
10	1.91533	50	2.22259
20	1.95374	60	2.36342
30	2.01775	70	2.52985

The measured and evaluated temperature changes are shown in Fig. 5(c). Here, the experimental data represents the liquid core temperature change, namely the changes of temperature difference under different angles. The data is recorded from maximum contact angle 69°. This maximum contact angle ensures the spring effect within the linear range. The theoretical temperature changes at four angles are displayed using red dots. Although there is an order of magnitude difference between the measured and evaluated temperature change, the trends are similar. The discrepancy might be caused by the distance between the meniscus and microbubble, the small evaporation area and simplification of the model [42]. The temperature change between contact angle ~10° and 0° can be clearly distinguished in the experiment. Combined with model estimation, we can determine that the measurement resolution of our sensor is below the order of 10^{-3} °C. In order to characterize the temperature resolution of this system, the standard deviation of temperature during the flat meniscus is 4.9×10^{-4} °C (see APPENDIX C for more details). The difference between the measurement temperature resolution and the estimated value may be due to the influence of complex parameters in the entire system and surrounding environmental fluctuations. To our knowledge, this is the first time to actually measure the order of 10^{-4} °C temperature fluctuate by the microcavity sensors. In the future, sensor packaging methods can be used to inprove the mechanical stability, such as 3-D printed packaged substrate [47] or spot-packaged method [48]. Furthermore, phone-sized microcavity sensing system [49] can further improve the robustness for practical applications.

III. Conclusion

In summary, an ultra-high resolution temperature sensor based on dual sensitization enhancement microbubble is demonstrated. The temperature response of optical WGM in microbubble is improved by injecting high thermo-optic coefficient liquid. The overall damping rate change and spring effect in optomechanics are observed in liquid core microbubble. The spring effect is sensitively related to laser cavity detuning and transfers the amplified optical response to the mechanical frequency shift. This dual amplification achieves an ultra-high sensitivity 8.1 MHz/°C, which is at least 2 orders of magnitude higher than that of conventional optomechanical approaches. The estimated temperature resolution is 5.3×10^{-5} °C. An ethanol evaporation experiment is constructed to demonstrate the actual temperature resolving ability. The measurement resolution of this system is 4.9×10^{-4} °C. The proposed method can be extended to other microcavity structured sensors and has great potential in ultra-high resolution sensing.

Appendix A: Liquid-core microbubble WGM and its temperature response characteristic

The microbubble cavity can support WGM resonance, and its resonant mode can be expressed as:

$$2\pi n_{\mathrm{eff}} R_1 = m\lambda_m \tag{A1}$$

where R_1 is the microbubble outer radius, n_{eff} is the corresponding effective refractive index, m is a positive integer representing the number of WGM angular modes. λ is the WGM resonant wavelength. The temperature induced WGM wavelength shift $d\lambda$ can be expressed as [17, 18]

$$\frac{d\lambda}{\lambda} = \alpha dT + \frac{\partial n_{eff}}{\partial T}\frac{1}{n_{eff}}dT \tag{A2}$$

the first term represents material thermal expansion coefficient, $\alpha = \frac{\partial R_1}{\partial T}\frac{1}{R_1}$. The second term is thermo-optic coefficient, and the effective refractive index change rate is:

$$\frac{\partial n_{eff}}{\partial T} = k_{core}\frac{\partial n_{eff}}{\partial n_{core}} + k_{wall}\frac{\partial n_{eff}}{\partial n_{wall}} + k_{air}\frac{\partial n_{eff}}{\partial n_{air}} + \alpha_{wall}\frac{\partial n_{eff}}{\partial t} \tag{A3}$$

where n_{core}, n_{wall} and n_{air} are the refractive indices of liquid core inside cavity, silica wall and air outside cavity, respectively. k_{core}, k_{wall} and k_{air} are their thermo-optic coefficients, respectively. t is the wall thickness. Since k_{air} and α_{wall} are relatively small, the last two terms can be ignored. Finally, the resonance wavelength temperature sensitivity can be obtained as:

$$S_T = \frac{d\lambda}{dT} = \lambda(\alpha + \frac{k_{core}}{n_{eff}}\frac{\partial n_{eff}}{\partial n_{core}} + \frac{k_{wall}}{n_{eff}}\frac{\partial n_{eff}}{\partial n_{wall}}) \tag{A4}$$

where $\alpha = 5\times10^{-7}\,℃^{-1}$, $k_{wall} = 11\times10^{-7}\,℃^{-1}$, $n_{wall} = 1.45$ for silica material. k_{core} and n_{core} are related to the injection solution. The wall has a positive thermo-optic coefficient and a positive thermal expansion coefficient. However, when the liquid core of the microbubble is acetone, the thermo-optic coefficient is negative. $k_{core} = -5.4\times10^{-4}\,℃^{-1}$ and $n_{core} = 1.43$. The effect of the liquid core thermo-optic coefficient is two orders of magnitude larger than the silicon influence, so the joint action of three factors will make the resonance wavelength produce blue shift. More importantly, the temperature sensitivity of the liquid core is also enhanced compared to the hollow microbubble.

Appendix B: The optomechanical oscillation and spring effect in the microcavity

In most optomechnical systems, the radiation pressure caused by the circulating optical power produces a radial force on the microresonator structure and causes deformation. Consequently, the mechanical displacement modulates the microcavity resonant frequency. This commonly coupling of dispersive nature is originated from the dependence of position and frequency and leads to several phenomena, such as the dynamic back-action and the optical spring effect. The theoretical framework of a purely dispersive interaction system has been studied for whisper gallery mode resonators [33, 34].

It can be understood through the coupled equations of motion for the cavity field amplitude and the mechanical amplitude:

$$\dot{A}(t)+A(t)[\frac{\kappa}{2}-i\Delta\omega(t)]=\sqrt{\kappa_{ex}}A_{in}$$

$$\ddot{x}+\Gamma_m\dot{x}+\Omega_m^2 x=\frac{f(t)}{m_{eff}}=\frac{2\pi|A(t)|^2 n/c}{m_{eff}} \quad \text{(B1)}$$

$$\Delta\omega(t)=(\Delta\omega_0+Gx)=(\Delta\omega_0+\frac{\omega x}{a})$$

where κ is the overall cavity intensity decay rate, from input (κ_{ex}) coupling and intrinsic (κ_o) losses, A_{in} is the input pump field (normalized such that $|A_{in}|^2$ is input power). m_{eff} is the effective microbubble mass, Γ_m is the mechanical damping rate, Ω_m is the intrinsic resonance frequency, f is the horizontal force applied by action of radiation pressure. For the wavelength difference (between the input beam and the moving-cavity resonance) $\Delta\omega(t)$, $\Delta\omega_0$ is the preset offset between cavity resonance ω_0 (when no light is input) and the input pump beam at frequency ω. G is optical frequency shift per displacement $G=\partial\omega_{cav}/\partial x$.

For a constant power CW laser input, the dynamic backaction between the cavity circulating light and mechanical motion changes the characteristics of the mechanical mode, resulting in an effective mechanical damping rate and an effective mechanical frequency change [30, 50]:

$$\Gamma_{opt}(\omega)=g^2\frac{\Omega_m}{\omega}[\frac{\kappa}{(\Delta\omega_0+\omega)^2+\kappa^2/4}-\frac{\kappa}{(\Delta\omega_0-\omega)^2+\kappa^2/4}] \quad \text{(B2)}$$

$$\delta\Omega_m(\omega)=g^2\frac{\Omega_m}{\omega}[\frac{\Delta\omega_0+\omega}{(\Delta\omega_0+\omega)^2+\kappa^2/4}+\frac{\Delta\omega_0-\omega}{(\Delta\omega_0-\omega)^2+\kappa^2/4}] \quad \text{(B3)}$$

Equation B2 shows the effect of the optomechanical damping rate. The full effective mechanical damping rate of system is $\Gamma_{eff}=\Gamma_m+\Gamma_{opt}(\omega)$. Since $\Gamma_{opt}(\omega)$ can be both positive and negative, it can either increase or decrease the mechanical damping rate. In the blue detuning situation ($\Delta\omega_0>0$), it is an amplification process. So, a narrowed mechanical linewidth can be observed. Equation B3 demonstrates the spring effect in the optomechanical system. The mechanical frequency depends sensitively on the laser cavity detuning. So, the resonant peak shift caused by temperature change can be transduced to the mechanical frequency change.

APPENDIX C: THE EXPERIMENTAL SETUP OF ETHANOL EVAPORATION

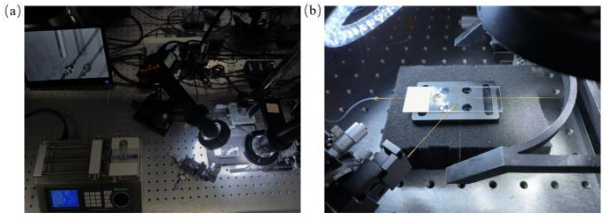

Fig. C1. Photos of the ethanol evaporation system.

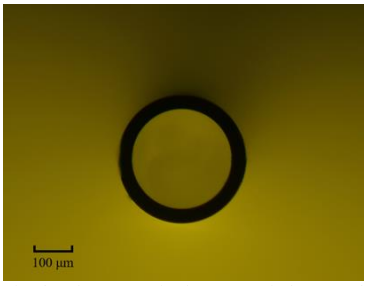

Fig. C2. Optical microscopic image of the used microtubule cross section.

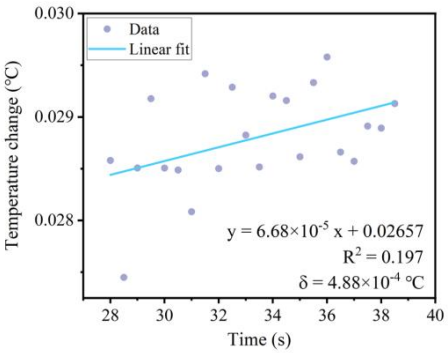

Fig. C3. The standard deviation δ of temperature during the flat meniscus.

REFERENCES

[1] H. Liang *et al.*, "A Lanthanide Upconversion Nanothermometer for Precise Temperature Mapping on Immune Cell Membrane," *Nano Lett,* vol. 22, no. 22, pp. 9045-9053, Nov 23 2022, doi: 10.1021/acs.nanolett.2c03392.

[2] K. Toutouzas *et al.*, "Elevated plaque temperature in non-culprit de novo atheromatous lesions of patients with acute coronary syndromes," *J Am Coll Cardiol,* vol. 47, no. 2, pp. 301-6, Jan 17 2006, doi: 10.1016/j.jacc.2005.07.069.

[3] J. Y. Jing *et al.*, "Performance improvement approaches for optical fiber SPR sensors and their sensing applications," (in English), *Photonics Res,* vol. 10, no. 1, pp. 126-147, Jan 1 2022, doi: 10.1364/Prj.439861.

[4] L. H. J. Raijmakers, D. L. Danilov, R. A. Eichel, and P. H. L. Notten, "A review on various temperature-indication methods for Li-ion batteries," (in English), *Appl Energ,* vol. 240, pp. 918-945, Apr 15 2019, doi: 10.1016/j.apenergy.2019.02.078.

[5] P. M. Fulton *et al.*, "Low coseismic friction on the Tohoku-Oki fault determined from temperature measurements," *Science,* vol. 342, no. 6163, pp. 1214-7, Dec 6 2013, doi: 10.1126/science.1243641.

[6] J. P. Abraham *et al.*, "A Review of Global Ocean Temperature Observations: Implications for Ocean Heat Content Estimates and Climate Change," (in English), *Rev Geophys,* vol. 51, no. 3, pp. 450-483, Sep 2013, doi: 10.1002/rog.20022.

[7] T. H. Kim *et al.*, "Kinetics of Magnetic Skyrmion Crystal Formation from the Conical Phase," *Nano Lett,* vol. 21, no. 13, pp. 5547-5554, Jul 14 2021, doi: 10.1021/acs.nanolett.1c00923.

[8] J. Sanjuan, A. Lobo, M. Nofrarias, J. Ramos-Castro, and P. J. Riu, "Thermal diagnostics front-end electronics for LISA Pathfinder," *Rev Sci Instrum,* vol. 78, no. 10, p. 104904, Oct 2007, doi: 10.1063/1.2800776.

[9] Y. G. Gong, J. Luo, and B. Wang, "Concepts and status of Chinese space gravitational wave detection projects," (in English), *Nat Astron,* vol. 5, no. 9, pp. 881-889, Sep 2021, doi: 10.1038/s41550-021-01480-3.

[10] C. Ling, J. Li, Y. P. Wang, H. Y. Chen, L. Y. Gu, and Y. W. Ding, "Structure optimization of a liquid-sealed SNS fiber optic temperature sensor," (in English), *Opt Laser Technol,* vol. 162, Jul 2023, doi: ARTN 109290
10.1016/j.optlastec.2023.109290.
[11] J. A. Lipa, J. A. Nissen, D. A. Stricker, D. R. Swanson, and T. C. P. Chui, "Specific heat of liquid helium in zero gravity very near the lambda point," (in English), *Phys Rev B,* vol. 68, no. 17, Nov 2003, doi: ARTN 174518
10.1103/PhysRevB.68.174518.
[12] K. J. Vahala, "Optical microcavities," *Nature,* vol. 424, no. 6950, pp. 839-46, Aug 14 2003, doi: 10.1038/nature01939.
[13] T. Carmon, L. Yang, and K. Vahala, "Dynamical thermal behavior and thermal self-stability of microcavities," *Opt. Express,* vol. 12, no. 20, pp. 4742-50, Oct 4 2004, doi: 10.1364/opex.12.004742.
[14] I. M. White and X. Fan, "On the performance quantification of resonant refractive index sensors," *Opt Express,* vol. 16, no. 2, pp. 1020-8, Jan 21 2008, doi: 10.1364/oe.16.001020.
[15] C. H. Dong *et al.*, "Fabrication of high-Q polydimethylsiloxane optical microspheres for thermal sensing," (in English), *Appl Phys Lett,* vol. 94, no. 23, Jun 8 2009, doi: Artn 231119
10.1063/1.3152791.
[16] C. H. He *et al.*, "Temperature sensor based on high-Q polymethylmethacrylate optical microbubble," (in English), *Laser Phys,* vol. 28, no. 7, Jul 2018, doi: ARTN 076202
10.1088/1555-6611/aab452.
[17] J. M. Ward, Y. Yang, and S. N. Chormaic, "Highly Sensitive Temperature Measurements With Liquid-Core Microbubble Resonators," (in English), *Ieee Photonic Tech. L.,* vol. 25, no. 23, pp. 2350-2353, Dec 1 2013, doi: 10.1109/Lpt.2013.2283732.
[18] Z. Liu *et al.*, "Whispering gallery mode temperature sensor of liquid microresonastor," *Opt Lett,* vol. 41, no. 20, pp. 4649-4652, Oct 15 2016, doi: 10.1364/OL.41.004649.
[19] Y. Wang, H. Li, L. Zhao, Y. Liu, S. Liu, and J. Yang, "Tapered optical fiber waveguide coupling to whispering gallery modes of liquid crystal microdroplet for thermal sensing application," *Opt Express,* vol. 25, no. 2, pp. 918-926, Jan 23 2017, doi: 10.1364/OE.25.000918.
[20] Y. Z. Yan *et al.*, "Packaged silica microsphere-taper coupling system for robust thermal sensing application," *Opt Express,* vol. 19, no. 7, pp. 5753-9, Mar 28 2011, doi: 10.1364/OE.19.005753.
[21] B.-B. Li, L. Ou, Y. Lei, and Y.-C. Liu, "Cavity optomechanical sensing," *Nanophotonics,* vol. 10, no. 11, pp. 2799-2832, 2021, doi: 10.1515/nanoph-2021-0256.
[22] K. H. Kim *et al.*, "Cavity optomechanics on a microfluidic resonator with water and viscous liquids," (in English), *Light-Sci. Appl.,* vol. 2, Nov 2013, doi: ARTN e110
10.1038/lsa.2013.66.
[23] E. Gil-Santos *et al.*, "High-frequency nano-optomechanical disk resonators in liquids," *Nat Nanotechnol,* vol. 10, no. 9, pp. 810-6, Sep 2015, doi: 10.1038/nnano.2015.160.
[24] M. Hossein-Zadeh, H. Rokhsari, A. Hajimiri, and K. J. Vahala, "Characterization of a radiation-pressure-driven micromechanical oscillator," *Physical Review A,* vol. 74, no. 2, 2006, doi: 10.1103/PhysRevA.74.023813.
[25] Y. Liu *et al.*, "Ultrahigh‐Resolution Optical Fiber Thermometer Based on Microcavity Opto‐Mechanical Oscillation," *Advanced Photonics Research,* vol. 3, no. 9, 2022, doi: 10.1002/adpr.202200052.
[26] G. Bahl, X. D. Fan, and T. Carmon, "Acoustic whispering-gallery modes in optomechanical shells," (in English), *New J Phys,* vol. 14, Nov 27 2012, doi: Artn 115026
10.1088/1367-2630/14/11/115026.
[27] F. Liu, S. Alaie, Z. C. Leseman, and M. Hossein-Zadeh, "Sub-pg mass sensing and measurement with an optomechanical oscillator," *Opt Express,* vol. 21, no. 17, pp. 19555-67, Aug 26 2013, doi: 10.1364/OE.21.019555.
[28] K. Zhu, K. Han, T. Carmon, X. Fan, and G. Bahl, "Opto-acoustic sensing of fluids and bioparticles with optomechanofluidic resonators," (in English), *Eur Phys J-Spec Top,* vol. 223, no. 10, pp. 1937-1947, Sep 2014, doi: 10.1140/epjst/e2014-02237-4.
[29] F. Pan *et al.*, "Radiation-Pressure-Antidamping Enhanced Optomechanical Spring Sensing," (in English), *Acs Photonics,* vol. 5, no. 10, pp. 4164-4169, Oct 2018, doi: 10.1021/acsphotonics.8b00968.
[30] W. Yu, W. C. Jiang, Q. Lin, and T. Lu, "Cavity optomechanical spring sensing of single molecules," *Nat Commun,* vol. 7, p. 12311, Jul 27 2016, doi: 10.1038/ncomms12311.
[31] J. Jiang *et al.*, "Wall-thickness-controlled microbubble fabrication for WGM-based application," *Appl Opt,* vol. 59, no. 16, pp. 5052-5057, Jun 1 2020, doi: 10.1364/AO.391545.
[32] V. Kavungal, G. Farrell, Q. Wu, A. K. Mallik, and Y. Semenova, "A Packaged Whispering Gallery Mode Strain Sensor Based on a Polymer-Wire Cylindrical Micro Resonator," (in English), *J Lightwave Technol,* vol. 36, no. 9, pp. 1757-1765, May 1 2018, doi: 10.1109/Jlt.2017.2784678.
[33] T. J. Kippenberg and K. J. Vahala, "Cavity opto-mechanics," *Opt Express,* vol. 15, no. 25, pp. 17172-205, Dec 10 2007, doi: 10.1364/oe.15.017172.
[34] T. Carmon, H. Rokhsari, L. Yang, T. J. Kippenberg, and K. J. Vahala, "Temporal behavior of radiation-pressure-induced vibrations of an optical microcavity phonon mode," *Phys. Rev. Lett.,* vol. 94, no. 22, p. 223902, Jun 10 2005, doi: 10.1103/PhysRevLett.94.223902.
[35] V. B. Braginsky, S. E. Strigin, and S. P. Vyatchanin, "Parametric oscillatory instability in Fabry-Perot interferometer," (in English), *Phys Lett A,* vol. 287, no. 5-6, pp. 331-338, Sep 3 2001, doi: Doi 10.1016/S0375-9601(01)00510-2.
[36] N. M. Hanumegowda, C. J. Stica, B. C. Patel, I. White, and X. D. Fan, "Refractometric sensors based on microsphere resonators," (in English), *Appl Phys Lett,* vol. 87, no. 20, Nov 14 2005, doi: Artn 201107
10.1063/1.2132076.
[37] K. Han, J. H. Kim, and G. Bahl, "Aerostatically tunable optomechanical oscillators," *Opt Express,* vol. 22, no. 2, pp. 1267-76, Jan 27 2014, doi: 10.1364/OE.22.001267.
[38] R. Luo, H. Jiang, H. Liang, Y. Chen, and Q. Lin, "Self-referenced temperature sensing with a lithium niobate microdisk resonator," *Opt Lett,* vol. 42, no. 7, pp. 1281-1284, Apr 1 2017, doi: 10.1364/OL.42.001281.
[39] Y. Wang, H. Y. Li, L. Y. Zhao, Y. J. Liu, S. Q. Liu, and J. Yang, "Tunable whispering gallery modes lasing in dye-doped cholesteric liquid crystal microdroplets," (in English), *Appl Phys Lett,* vol. 109, no. 23, Dec 5 2016, doi: Artn 231906
10.1063/1.4971973.
[40] J. Polansky and T. Kaya, "An experimental and numerical study of capillary rise with evaporation," (in English), *Int J Therm Sci,* vol. 91, pp. 25-33, May 2015, doi: 10.1016/j.ijthermalsci.2014.12.020.
[41] C. Buffone, C. Minetti, L. Boussemaere, M. Roudgar, and J. De Coninck, "Marangoni convection in evaporating meniscus with changing contact angle," (in English), *Exp Fluids,* vol. 55, no. 10, Oct 2014, doi: ARTN 1833
10.1007/s00348-014-1833-2.
[42] C. Buffone, K. Sefiane, and J. Christy, "Infra-Red measurements of an evaporating meniscus with imposed contact angle," (in English), *Int J Therm Sci,* vol. 121, pp. 89-98, Nov 2017, doi: 10.1016/j.ijthermalsci.2017.07.005.
[43] C. Buffone, K. Sefiane, and J. R. E. Christy, "Experimental investigation of self-induced thermocapillary convection for an evaporating meniscus in capillary tubes using micro–particle image velocimetry," *Physics of Fluids,* vol. 17, no. 5, 2005, doi: 10.1063/1.1901688.
[44] A. Cecere, C. Buffone, and R. Savino, "Self-induced Marangoni flow in evaporating alcoholic solutions," (in English), *Int J Heat Mass Tran,* vol. 78, pp. 852-859, Nov 2014, doi: 10.1016/j.ijheatmasstransfer.2014.07.055.
[45] C. Buffone and K. Sefiane, "Temperature measurement near the triple line during phase change using thermochromic liquid crystal thermography," (in English), *Exp Fluids,* vol. 39, no. 1, pp. 99-110, Jul 2005, doi: 10.1007/s00348-005-0986-4.
[46] H. Hu and R. G. Larson, "Evaporation of a Sessile Droplet on a Substrate," *The Journal of Physical Chemistry B,* vol. 106, no. 6, pp. 1334-1344, 2002, doi: 10.1021/jp0118322.
[47] J. Liao and L. Yang, "Optical whispering-gallery mode barcodes for high-precision and wide-range temperature measurements," *Light: Science & Applications,* vol. 10, no. 1, 2021, doi: 10.1038/s41377-021-00472-2.

[48] Y. Z. Yan *et al.*, "Robust Spot-Packaged Microsphere-Taper Coupling Structure for In-Line Optical Sensors," (in English), *Ieee Photonic Tech L,* vol. 23, no. 22, pp. 1736-1738, Nov 15 2011, doi: 10.1109/Lpt.2011.2169051.

[49] X. Y. Xu, W. J. Chen, G. M. Zhao, Y. H. Li, C. Y. Lu, and L. Yang, "Wireless whispering-gallery-mode sensor for thermal sensing and aerial mapping," (in English), *Light-Sci Appl,* vol. 7, Sep 12 2018, doi: ARTN 62
10.1038/s41377-018-0063-4.

[50] M. Aspelmeyer, T. J. Kippenberg, and F. Marquardt, "Cavity optomechanics," *Reviews of Modern Physics,* vol. 86, no. 4, pp. 1391-1452, 2014, doi: 10.1103/RevModPhys.86.1391.